Environmental Science Nano

Accepted Manuscript

ROYAL SOCIETY OF CHEMISTRY

rsc.li/es-nano

Nano Impact Statement

To address the biofouling problem associated with thin film composite (TFC) forward osmosis (FO) membranes, we have developed novel surface coatings through covalent bonding of silver decorated graphene oxide (GO/Ag).

GO/Ag nanocomposite functionalization of TFC FO membranes provides an effective antimicrobial surface that has better characteristics than either GO or AgNPs independently. This enhanced effectiveness likely results from the synergistic effect of the capture-killing mechanism displayed by this system. In addition, the higher hydrophilicity of the resulting membranes, the low material cost, and the ease of preparation (dip coating method) result in an effective approach than other modification methods. Finally, using graphene oxide as a support for biocidal metal nanoparticles provides an opportunity for the regeneration of biocidals after release

Surface Modification of Thin Film Composite Forward Osmosis Membrane by Silver-Decorated Graphene-Oxide Nanosheets

Environmental Science: Nano

Revised: June 27, 2015

Adel Soroush, Wen Ma, Yule Silvino, Md. Saifur Rahaman*

Department of Building, Civil and Environmental Engineering, Concordia University

1455 de Maisonneuve Blvd. West, EV-6.139, Montreal, Quebec, Canada, H3G 1 M8

*Corresponding author. Tel.: +15148482424, Ext. 5058

E-mail address: saifur.rahaman@concordia.ca (M.S. Rahaman)

ABSTRACT

Forward osmosis (FO), as an emerging technology for seawater desalination and wastewater reuse, has been attracting significant interest because of its energy efficiency. However, membrane fouling represents one of the major limitations for this technology, notably for thin film composite (TFC) polyamide (PA) membranes, which are prone to chlorine attack. In this study, silver nanoparticle (AgNP)-decorated graphene oxide (GO) nanosheets (as an effective biocidal material) were covalently bonded to the PA surface to impart improved hydrophilicity and antibacterial properties to the membrane. AgNPs were synthesized in situ by the wet chemical reduction of silver nitrate onto the surface of GO nanosheets. The formation of the composite was verified by UV-Vis spectroscopy, x-ray diffraction, and transmission electron microscopy techniques. The synthesized GO/Ag nanocomposites were then covalently bonded onto the TFC PA membrane surface using cysteamine through an amide forming condensation reaction. ATR-FTIR and XPS results confirmed the covalent bonding of the nanocomposite onto the TFC PA surface. Overall, the GO/Ag nanocomposite functionalized membranes exhibited super-hydrophilic properties (contact angles below 25°) and significant bacterial (*E. coli*) inactivation (over 95% in static bacterial inactivation tests) without adversely affecting the membrane transport properties.

INTRODUCTION

Forward osmosis (FO) has recently been considered to be a promising technological approach for seawater desalination and water reuse because of the energy efficiency of the overall process of water separation[1, 2]. Although the FO process is less prone to fouling than reverse osmosis (RO), membrane fouling (notably biofouling) remains one of the important limitations to widespread application[3]. Thin film composite polyamide (PA) FO membranes are highly susceptible to biofouling because of their intrinsic physicochemical surface properties[4]. Although using oxidizing agents is a common method for controlling biofouling[5, 6], other alternative methods must be considered because PA layers are sensitive to chemical oxidation and degrade in the presence of common disinfectants.

Membrane surface modification is one of the well investigated methods for preventing biofilm formation[7]. Different methods of surface modification have been reported[3, 8] including grafting

macromolecules[9-12], preparing antifouling surfaces by functionalization[13] with photocatalytic NPs such as TiO_2[14, 15] and carbon-based nanomaterials,[16, 17] and using biocidal NPs such as silver (Ag) NPs either incorporated into the support layer[18, 19]or attached to the surface of the TFC membranes[20]. Problems associated with using biocidal NPs are their tendency toward agglomeration and detachment from the surface, releasing into the water. One of the best approaches to overcoming such problems is to use carbon-based nanocomposites (instead of using a single type of NPs)[21].

Graphene oxide (GO), as a single-atomic-thick sheet consisting of hydrophilic oxygenated functional groups in the form of carboxyl, hydroxyl, ether, and epoxy, has attracted interest in different scientific areas[22, 23]. Several intrinsic characteristics of GO nanosheets, such as their smoothness, atomic-level thickness, high water slip length, and low cost of bulk production through the chemical oxidation of graphite, establish potential new applications in water purification[24-26]. Furthermore, specific efforts have investigated using GO to improve membrane durability by preventing the attachment of hydrophobic foulants or by forming a protective layer against chlorine attack[27]. Because of its highly functionalized basal planes and edges, GO presents special features when used as a support for noble metal nanoparticles such as gold (Au) and silver (Ag). Au and Ag are widely used as sensors or catalysts[28] in electrical and environmental applications. Ag-decorated GO nanocomposites have been established as a new type of effective, easily synthesized, and cost effective biocidal materials in health and environmental applications[29-31]. GO nanosheets, employed to stabilize Ag nanoparticles and enhance the contact between Ag and bacteria, result in a synergetic effect for these new nanocomposites[32]. Although there are some studies suggesting special core-shell[33] or nanoscrolls structure[30], based on different silver salt and chemical reductant or post-synthesizing procedure, majority of GO/Ag nanocomposite morphologies provide a very well-distributed silver decoration.

AgNPs are well studied for their enhancement of antifouling properties; for instance, Rahaman *et al.* used the combination of AgNPs with polymer brushes to prepare antifouling TFC RO membranes[34]. Yin *et al*. covalently bonded AgNPs onto the surface of TFC RO membranes to reduce membrane biofouling[20], and Mauter *et al*. grafted AgNPs irreversibly onto the ultrafiltration (UF) membrane surface with a high silver release capacity[35]. The two major

problems in using AgNPs for the surface modification of membranes are the high tendency of these NPs to agglomerate, leading to insufficient contact with bacteria, and the instability of the NPs on the membrane surface[36-38]. However, only a handful of studies investigated incorporating GO nanosheets on the membrane surface, either by electrostatic attraction or covalent bonds between GO and TFC RO membranes. Choi *et al*. used a layer-by-layer assembly of GO nanosheets on TFC RO membranes to protect these membranes against chemical degradation resulting from chlorine attack. Perreault *et al*. covalently bonded GO to the surface of TFC RO membranes and reported an increase in the hydrophilicity and antibacterial properties (~65% inactivation of bacteria) of the membranes[39]. However, neither AgNP nor GO alone can exploit their full potential in controlling membrane biofouling. Therefore, novel composite materials of individual nanomaterials are required to fully develop their potential for biofouling mitigation. In this manuscript, we use composite GO nanosheets and AgNPs as a new and promising class of biocidal materials for membrane surface modification.

In this study, silver-decorated GO nanosheets are used to functionalize PA TFC membranes. Silver-decorated GO nanocomposites were prepared through wet chemical reduction and covalently bonded to the surface of TFC FO membranes. TFC membranes were first chemically treated by cysteamine through a click chemistry reaction. Unreacted acyl chloride groups from the interfacially polymerized PA layer and amine groups of the cysteamine formed amide bonds. The thiol groups of cysteamine then reacted with the as-prepared silver decorated GO nanosheets. The results of this study show the synergetic effect of the combination of GO nanosheets and AgNPs in the inactivation of bacteria without any adverse effects on membrane transport properties. This finding highlights a novel path for establishing a new class of biocidal materials.

MATERIALS AND METHODS

Materials.

The following chemicals were used as received: silver nitrate (99.9999% on a trace metal basis, Sigma-Aldrich), ethanol (Sigma-Aldrich), cysteamine (95%, Sigma-Aldrich), and sodium borohydride (99.99%, Sigma-Aldrich). De-ionized (DI)-water was prepared in a Millipore Milli-

Q purification system. The TFC FO membranes were obtained from Hydration Technology Innovation, LLC and were soaked in a DI-water bath for 24 hours prior to modification.

Synthesis and Characterization of AgNPs and GO/Ag Nanocomposites.

Graphene oxide (GO) nanosheets were purchased from Cheap Tubes Inc. (Grafton, VT, USA); these nanosheets were synthesized by a modified Hummers method[40]. The single layer sheets were 0.7-1.2 nm thick and displayed a size distribution of 300-800 nm. The GO nanosheets were decorated with silver (Ag) through an in situ reduction of silver nitrate on the surface. The GO (50 mg) was dispersed in 100 mL of DI water through probe sonication (Branson 3510) for 1 h at 70% of the maximum power output. In total, 100 mL of silver nitrate solution (20 mM) was prepared and added to the GO suspension. The resulting mixture was mixed at room temperature for 30 min, and 10 mL of a sodium borohydride solution (5 mM) was added dropwise. Mixing continued for 5 h to complete the formation of AgNPs. Over time, the reaction mixture changed from a dark brown to a grayish color. The resulting GO/Ag nanocomposite mixture was centrifuged for 15 min at 12,500 rpm, rinsed with DI water three times and dried overnight in an oven at 80°C. The formation of GO/Ag nanocomposites was evaluated by UV-Vis absorption spectroscopy (UV-Vis LAMDA650, Perkin Elmer), X-ray diffraction (XRD Philips PW1710), thermal gravimetric analysis (TGA Q5000 V3.15 Build 263), and high-resolution transmission electron microscopy (HRTEM Tecnai G2 F20). Further characterization of the nanocomposite was accomplished using Raman and attenuated total reflectance-Fourier transform infrared (ATR-FTIR) spectroscopy techniques.

Surface Modification and Characterization of TFC FO Membranes.

TFC FO membranes were purchased from Hydration Technology Innovation (HTI) and were functionalized with GO/Ag nanocomposites using a cysteamine solution (Scheme 1). Unreacted acyl halide groups on the surface of TFC polyamide membranes reacted with the amine functional group of cysteamine through a click chemistry reaction and formed strong amide bonds, providing the membrane surface with thiol functionality for subsequent covalent bonding

of GO/Ag nanocomposites onto the membrane surface. TFC membranes were cut and placed on a glass plate and covered with a frame; only the active side was exposed to the cysteamine solution. Frames were clamped with clips to prevent any leakage. The entire assembly was then placed on an orbital shaker, rotating at 70 rpm at room temperature. Membranes were immersed in a cysteamine ethanol solution (20 mM) for 30 min and were then removed, rinsed with DI water three times, and immersed in the as-prepared GO/Ag nanocomposite suspension for 12 h. The resulting functionalized membranes were then washed with DI water three times and were refrigerated (4°C) until use.

The intrinsic membrane transport properties (e.g., water permeability and salt permeability) were evaluated in RO cross-flow cell based on standard methodology for evaluating membrane performance in osmotically driven membrane processes[41]. The permeation cell was designed to provide an effective surface area of 42.75 cm^2. The membrane was compacted overnight with DI water at 70 psi until a steady water permeate flux was reached. In the RO mode in the experiment, the water flux (J) and water permeability (A) of the membranes were evaluated using the following equations:

$$J = \frac{\Delta V}{A_m \Delta t} \qquad (1)$$

$$A = \frac{J}{\Delta P} \qquad (2)$$

where A_m is the effective membrane surface area, ΔV is the collected permeate volume during Δt and ΔP is the applied pressure difference.

The salt rejection was determined by measuring the rejection of a 50 mM NaCl solution using a calibrated conductivity meter (Oakton Instruments, Vernon Hills, IL, USA). The salt rejection of the membranes was calculated using the following equation:

$$R = \left(1 - \frac{C_p}{C_f}\right) \times 100\% \qquad (3)$$

where C_p and C_f are the salt concentrations in the permeate and feed solutions. The salt concentrations were determined by measuring the conductivity of the solution using a calibrated conductivity meter. The salt permeability coefficient (B) was calculated as follows:

$$\frac{1-R}{R} = \frac{B}{A(\Delta P - \Delta\pi)} \qquad (4)$$

where A is the water permeability, ΔP is the transmembrane pressure, Δπ is the osmotic pressure of the feed solution and R is the salt rejection.

The membrane performance in the FO mode was also evaluated using a lab scale cross-flow cell with the same dimensions as the RO cell. Both the feed (DI water) and draw solution (1 M NaCl) were circulated at the same flow rate (0.2 L/min) and applied pressure. The temperature of the feed and draw solution was maintained constant at 25°C. To precisely measure the water flux, a digital analytical balance was employed to measure the weight change of the draw solution. The salt reverse flux of the membranes was calculated by measuring the conductivity of the draw solution before and after the FO process using a calibrated conductivity meter (Oakton Instruments, Vernon Hills, IL). The FO water flux (JV) and reverse salt flux (JS) were calculated as follows:

$$J_V = \frac{\Delta V}{A_m \Delta t} = \frac{\Delta m/\rho}{A_m \Delta t} \qquad (5)$$

$$J_S = \frac{\Delta(C_t V_t)}{A_m \Delta t} \qquad (6)$$

Where Δm is the weight change of the draw solution, Am is the effective surface area, and C_t and V_t are the salt concentration and volume of the feed solution after the process, respectively.

The elemental composition of the virgin and functionalized membranes was determined by X-ray photoelectron spectroscopy (XPS, SK-Alpha). Samples were irradiated with a beam of monochromatic Al K_α X-rays with an energy of 1.350 keV. Changes in the functional groups of the samples during the chemical reaction were studied using attenuated total reflectance-infrared spectroscopy (Nicolet 6700 / Smart iTR), which was conducted using a germanium crystal on desiccator-dried samples. The surface morphology of the membrane was observed by field-emission scanning electron microscopy (FE-SEM; JEOL, JSM-7600 TFE) to verify the presence of GO/Ag nanocomposite. Prior to imaging, the surface of the membranes was coated with a thin layer (15 nm) of carbon; the carbon was sputtered onto the layers by carbon evaporation (EDWARDS AUTO306). Roughness parameters of the membranes were determined using atomic force microscopy (AFM, Dimension 3100) in the tapping mode.

The surface hydrophilicity and surface energy of the membranes were evaluated through contact angle measurements of DI water using the sessile drop method (VCA, video contact angle system, AST Products, Inc., Billerica, MA, USA). The right and left angles of the water drop were measured using the system software (VCA optima XE). At least three desiccator-dried samples and approximately five points for each sample were selected for contact angle measurements. The data were averaged between the samples. The relative wettability of the membranes was evaluated by calculating the membrane-liquid interfacial free energy[42, 43] as

$$-\Delta G_{ML} = \gamma_L (1 + (\cos\theta)/r) \qquad (7)$$

where θ is the average contact angle, γ_L is the pure water surface tension (72.8 mJ/m^2 at 25° C) and r is the roughness area ratio (ratio of the actual surface to the planar surface area for rough materials, r = 1+ SAD; SAD is the surface area difference parameter obtained from AFM measurements).

The streaming potential of the virgin and functionalized membranes, as an indicator of membrane surface charge, was measured using an electrokinetic analyzer (EKA Anton Paar) at various pH values with a 1 mM KCl electrolyte solution. The procedure and calculations followed the method described by Walker *et al.* [44].

Scheme 1

Antimicrobial Activity of GO/Ag Functionalized Membranes.

Bacterial inactivation was evaluated by determining and comparing the number of viable bacteria present on surfaces of virgin and functionalized membranes through a simple plate counting method. Briefly, *Escherichia coli* (PGEN-GFP (LVA) ampR) was grown overnight at 37° C in Luria-Bertani (LB) broth medium. The bacterial solution was diluted and cultured for 2 h to reach the log phase and was verified by an optical density measurement at 600 nm. The resulting bacterial solution was centrifuged and washed three times with 0.9% saline solution before being diluted to 10^7 CFU mL^{-1} in 0.9% saline solution. For the exposure phase, 1.5 cm^{-2} membranes

were punched and placed in a plastic holder with the active layer facing the bacterial solution. The holders were maintained at room temperature for 1 h. After 1 h of incubation, the excess solution was discarded, and the membranes were washed with a sterile saline solution. To remove attached bacteria from the membrane surface, the membrane coupons were bath-sonicated for 7 min in a 10 mL isotonic solution. Finally, 100 µL serial dilutions (representing over 6 orders of magnitude) of the bacterial solution were spread on LB agar plates with ampicillin and incubated overnight at 37°C. The number of colonies was then counted.

Silver Release Experiments.

The reservoir method was used to measure the silver ion loading and releasing from GO/Ag functionalized membranes[35]. For ion releasing measurements, both the functionalized and virgin membrane samples were cut into 1 inch coupons and incubated in 20 mL of DI water for 24 h; the samples were then acidified with 1% HNO_3. The silver loading was conducted with a similar procedure, but the solution was acidified prior to incubation. Silver ion concentrations in the samples were then measured by inductively coupled plasma mass spectroscopy (ICP-MS Perkin Elmer NexION 300X). The ion release experiments for both the control and functionalized membrane were conducted for 6 days.

RESULTS AND DISCUSSION

Successful Graphene Oxide/ Silver Nanocomposite Synthesis Confirmed by UV-Vis, TEM, TGA and XRD Analyses.

The GO/Ag nanocomposite was synthesized through the in situ reduction of silver nitrate onto GO nanosheets and was characterized by UV-Vis, XRD, TGA and TEM (Figure 1). The UV-Vis spectra of GO, Ag nanoparticles, and GO/Ag suspension indicates the formation of a nanocomposite (Figure 1(A)). GO exhibits two different characteristic bands at 230 nm, corresponding to the electronic π-π^* transition of the C=C aromatic bond and a shadow shoulder at 305 nm assigned to the n-π^* of C=O bonds. Additionally, AgNPs exhibit a band at 400 nm in the absorption spectrum, which is attributed to a surface plasmon. The UV-Vis spectrum of GO/Ag shows both characteristic GO and Ag bands and verifies the formation of GO/Ag nanocomposites. The presence of AgNPs in the GO/Ag nanocomposite was also confirmed

through XRD measurements. GO/Ag XRD patterns (Figure 1(B)) represent the prominent Bragg peaks at 2θ values of 38.1°, 44.3°, 64.5°, and 77.5°, assigned to the (1 1 1), (2 0 0), (2 2 0) and (3 1 1) crystallographic planes of face-centered cubic (fcc) AgNPs, respectively. The peak at 2θ = 10.1° of GO nanosheets (attributed to the stacking of the GO layer) was completely removed because the anchoring of AgNPs on the surface of the GO sheets prevented the restacking of the layered structure of GO[31]. The formation of GO/Ag nanocomposite was also reflected in the TGA (Figure 1C). Graphene oxide exhibits a two-step decomposition. The first drop appears at 220°C and is attributed to the decomposition of labile oxygen containing functional groups, and the second drop occurs at 550°C and is attributed to the pyrolysis of the carbon skeleton of GO. However, AgNPs do not show a decomposition step in the TGA. For the GO/Ag nanocomposite, the combination of the two different behaviors is observed, and the mass ratio of GO and Ag can be estimated in the final composite.

The morphological features of the GO/Ag nanocomposite were investigated by HRTEM. TEM images revealed a well-dispersed layer of spherical AgNPs decorating the surface of the GO nanosheets (Figure 1D). The results indicate that GO plays a decisive role in the nucleation and growth of Ag nanoparticles, and the presence of GO and its functional groups act as a morphological driver/controller for silver NPs, preparing for the formation of the spherical NPs. The oxygen containing functionalities on the GO surface provides reactive sites for the nucleation and growth of AgNPs. However, the AgNPs synthesized without GO and without using any capping agent displayed an aggregated morphology (additional TEM images of GO, Ag NPs and GO/Ag nanocomposites are provided in the Supporting Information in Figure S2).

Figure 1.

Graphene Oxide/ Silver Nanocomposites were Covalently Bonded to the Surface of the TFC Polyamide Membrane.

The enhanced stability of the functionalized GO/Ag nanocomposite on the membrane surface was obtained using a cysteamine linker with amine and thiol functional groups at each end. The

amine group reacts with the un-reacted acyl chloride functional groups on the surface of the TFC membrane from interfacial polymerization. The presence of acyl chloride groups was verified by an elemental analysis using an XPS method on the surface of a pristine membrane. Cl2p has a peak of approximately 198 eV (Figure S5, supporting information), and the area below that peak is estimated to be approximately 1% Cl element by weight. XPS results for the cysteamine treated membrane also indicated that all acyl chlorides were consumed during the reaction, the Cl content of the surface became zero, and the new surface showed the presence of sulfur, which displays a peak at 162 eV (Figure S5, supporting information). The thiol groups on the membrane surface would react with and anchor AgNPs [45]. AFM images (Figures 2 (C) and (D)) reveal that after GO/Ag nanocomposites bonded onto the TFC membrane surface, both the surface roughness and surface morphology of the membrane significantly changed. The graphene oxide nanosheets flattened the surface of the membrane; therefore, the overall roughness decreased (Supporting information, Table S1). The SEM images further confirm the change in the morphology of the GO/Ag functionalized membrane surface when compared to pristine membranes (Figures 2 (A) and (B)). As shown in Figure 2B, the spherical AgNPs are distributed predominantly on the surface of the GO nanosheets and less on the edge or within the valley-like region of the TFC membrane surface. Higher contrast images of AgNPs and membrane surfaces were obtained using backscattered electron microscopy (BCE); the images are provided in the supporting information (Figure S1). The BCE images verified the presence and uniform distribution of AgNPs on the surface of GO and TFC membranes. The size and shape of the AgNPs observed also agreed with the TEM observations (Figure 1).

Figure 2.

The progress of the reaction was also studied using the ATR-FTIR method. The ATR-FTIR spectra in Figure 3C (details in the supporting information Figure S3) show that after treating the TFC membranes with cysteamine, the intensity of the peak at 850 cm^{-1} (C-Cl bond in the stretching mode) decreased, indicating the consumption of the acyl chloride group, and a new peak at 1020 cm^{-1} appeared, which can be attributed to the formation of a new aliphatic amine C-

N bond in the stretching mode. Additionally, the TFC membranes have two small peaks located at 1147 cm^{-1} and 1585 cm^{-1} that are assigned to the C-O-C stretching and the phenyl ring vibration of the polysulfone support layer, respectively. These results verify the binding of the GO/Ag nanocomposite onto the surface of the TFC membranes. A Raman spectroscopy analysis was conducted to characterize disordered carbonaceous materials such as GO nanosheets. In comparison with the virgin TFC FO membrane, which displays no characteristic peak in the Raman spectra, the GO/Ag is represented by two strong characteristic peaks at 1320 cm^{-1} (D band) and 1570 cm^{-1} (G band) with 532 nm laser excitation. The Raman spectroscopy results indicate the presence of the GO/Ag nanocomposites on the surface of the TFC FO membranes.

The physical stability of the GO/Ag nanocomposite bonded to the TFC membranes was evaluated through an XPS analysis. To investigate the role of GO in stabilizing the silver NPs on the membrane surface, the membranes functionalized with AgNPs (synthesis procedure is provided in supporting information) and GO/Ag nanocomposites were sonicated for 7 min, and the silver content of each membrane (after sonication) was estimated in an XPS analysis. Metallic Ag 3*d* peaks are centered at 373.9 and 367.9 eV, consistent with the reported values[46]. Although more Ag was loaded on the membranes decorated with Ag NPs than on GO/Ag functionalized membranes, the Ag loss by physical stress was enhanced by using GO as a support for Ag NPs. In total, 50 percent of the Ag NPs were lost during sonication, whereas only 6 percent were lost from GO/Ag functionalized membranes (Figure S6, supporting information).

Figure 3.

Membrane Transport Properties were not Significantly Affected by GO/Ag Functionalization.

The FO process is operated without applying any high transmembrane pressure. Therefore, any surface modification may influence the membrane permselectivity properties, unlike other pressure-driven membrane processes. The iIntrinsic transport properties of the membrane, *i.e.,*

pure water permeability (A) and salt permeability (B), were evaluated in a RO mode experiment. The water flux and reverse salt flux of a 1 M NaCl solution in the FO mode were also evaluated to determine the effect of GO/Ag nanocomposite functionalization on the performance of the TFC FO membrane. Both the pure water permeability (A) and salt permeability coefficient (B) of the functionalized TFC membrane did not significantly change from those of the control TFC membranes. The pure water permeability decreased by approximately 6%, and the salt permeability coefficient increased by 13% (Figure 4A). Because the cysteamine treatment has no adverse effect on the membrane performance[20], the change in pure water permeability and salt permeability coefficient can be attributed to the formation of a barrier layer of GO/Ag, which can hinder water flux. The water flux of TFC membranes in the FO mode slightly decreased after modification (2% decrease), and the value of the reverse salt flux increased by approximately 20% (Figure 4B). These changes may be attributed to the formation of an additional layer on the surface of the membrane, which may act as a barrier and decrease the water flux. Moreover, the

GO nanosheets possess frictionless surfaces which can affect the formation of an internal boundary layer, changing shear stresses and thus affecting membrane transport properties (since there is no external pressure applied in FO process). Also the presence of silver nanoparticles on the membrane surface, which can release positively charged Ag ions, can change the charge distribution and charge interactions between feed solution and membrane surfaces interface. These two factors can affect the membrane transport properties in FO mode.

According to the contact angle measurements, Figures 4C and 4D show the water contact angle of the membrane decreasing from 55° for the virgin TFC FO membrane to 24° for the functionalized membrane, indicating that the GO/Ag functionalization provides a highly hydrophilic surface. This change in hydrophilicity of the membrane with GO/Ag functionalization is attributed to the presence of hydrophilic oxygen-containing functional groups on the GO nanosheets. Additionally, the hydrophilicity is a critical factor for controlling the fouling of the FO membranes. The surface zeta potential, the type of charge, and the density of the exposed charge are the other crucial parameters that determine the fouling properties of the membrane. The observed zeta potential (Figure S4 in the supporting information) for a pristine TFC PA membrane agreed with the protonation behavior of polyamide functional groups. At a low pH, the unreacted amine groups remaining after the interfacial polymerization (characterized

by a broad peak at 3500 cm^{-1} in the ATR-FTIR spectra in Figure 3 (C)) were protonated, whereas the carboxylic groups remained unchanged. As the pH increased to a value above the pK_a of the carboxylic group, these groups were deprotonated, and the surface charge of the membrane became negative and remained constant[47]. By functionalizing the surface with GO/Ag nanocomposites, the protonation of the unreacted amine groups occurred in a similar manner when the pristine TFC membrane was immersed in a low pH solution. At higher pH values, however, numerous carboxylic groups were present on the surface of the GO nanosheets, and thus, deprotonation occurred to a higher extent than for pristine membranes. As a result, functionalized membranes impart more negative charges.

Figure 4.

The Functionalized Membrane Exhibited Strong Antimicrobial Activity.

As reported elsewhere, [48] microbial inactivation occurs through a three-step mechanism. The primary step is cell deposition onto the carbon-based nanomaterials. Similar to single-wall carbon nanotubes, graphene oxide inactivates bacteria by direct cell contact and membrane damage[49] and through charge transfer and formation of reactive oxygen species [50]. Silver nanoparticles also exhibit significant antimicrobial properties through different proposed mechanisms such as the following: *i*) releasing Ag^+ ions, which strongly bind to thiol groups in enzymes and proteins on the cellular surface and cause destabilization of the membrane and cellular walls; *ii*) attaching to the surface of the bacteria and producing holes in the membrane and cellular wall, allowing the AgNPs to penetrate into the bacteria; or *iii*) producing reactive oxygen species under oxidizing conditions that are capable of irreversibly damaging cellular DNA replication[50]. In the case of the GO/Ag nanocomposite, a synergetic phenomenon in bacterial inactivation is observed, which is called the capture-killing mechanism[48]. Graphene oxide plays an important role as a support for the AgNPs and prevents the AgNPs from agglomerating. The GO also dictates a spherical morphology to the AgNPs and thus provides a larger active surface area, a shape that results in higher antimicrobial activity. In addition, the graphene oxide displays the ability to capture bacteria on its surface[48, 51], which, for the GO/Ag

nanocomposite, results in a higher chance of bacterial inactivation by AgNPs. Additionally, graphene oxide can rupture the membrane wall because of its sharp edges[49, 52].

Using *E. coli* (GFP level 1) as a model organism, the antimicrobial activity of control and functionalized TFC membranes was investigated in static bacterial inactivation tests. The results show that even over a short period of contact (*i.e.,* 1 h), the GO/Ag nanocomposite functionalized membranes significantly reduced the number of viable *E. coli* cells by 96%, which is higher than that of either independent graphene oxide or AgNP functionalized membranes (Figure 5). To better understand the synergetic effects of the GO nanosheets and AgNPs in GO/Ag nanocomposites, TFC functionalized membranes with AgNPs and GO were prepared and examined in an antibacterial analysis. The results show significant differences in bacterial inactivation of the three modified membranes. Silver NP modified membranes displayed a 60% inactivation, whereas GO nanosheet functionalized membranes displayed an approximately 40% bacterial inactivation. Silver decorated graphene oxide showed a remarkably high inactivation (approximately 96%). These results can be attributed to a synergetic effect of the combination of silver NPs and graphene oxide, which have different approaches to bacterial inactivation. GO/Ag nanocomposites can inactivate bacteria not only through silver ions being released and penetrating into the cells[50] but also through the sharp edges of GO nanosheets rupturing the membrane wall[49]. The biocidal effect of cysteamine was also studied as a control sample. In comparison with the TFC membrane, a negligible biocidal effect was observed resulting from the cysteamine.

Silver Ion Release Behavior was Different for Composite and only AgNP Modified Membranes.

The silver ion loading and release behavior were analyzed by ICP-MS. To investigate the effect of the GO support on the release of AgNPs, AgNP decorated TFC membranes were compared with a GO/Ag functionalized membrane. The reactant concentration of AgNPs during synthesis was constant to allow for rational comparisons. The results show that the silver content for the AgNP decorated membranes (13.38 μg/L) was approximately three times greater than that for the GO/Ag decorated membrane (5 μg/L), agreeing with the XPS elemental composition. However, the release behavior of these two functionalized membranes was different. Whereas silver ions are released moderately over time for the AgNP decorated membrane, the release of

silver ions from the GO/Ag decorated membrane occurred immediately in the first day and remained constant with time (Figure 5 (B)). However, the bacterial inactivation results indicate that the GO/Ag decorated membranes were more effective compared with GO and AgNP functionalized membranes. These results indicate that the Ag decorated membranes can inactivate bacteria by releasing ions; however, the GO/Ag functionalized membranes can release ions and rupture cells because of the sharp edges of the GO nanosheets, enhancing the bacterial inactivation. The synergetic performances for the GO/Ag functionalized membrane can be attributed to the combined mechanisms of bacterial inactivation that have been engendered by the GO nanosheets and silver NPs. Although the results of this paper are comparable to other publications[34, 35] with regards to the silver loading and releasing rate, the earlier defined regeneration process should be incorporated for practical long-term real-world applications. Because the membrane is functionalized with GO, the regeneration process can be accomplished easily through the in situ synthesis of AgNPs (information regarding the membrane preparation is provided in the supporting information).

Figure 5.

CONCLUSIONS.

GO/Ag nanocomposite functionalization of TFC FO membranes provides an effective antimicrobial surface that has better characteristics than either GO or AgNPs independently. This enhanced effectiveness likely results from the synergistic effect of the capture-killing mechanism displayed by this system. In addition, the higher hydrophilicity of the resulting membranes, the low material cost, and the ease of preparation (dip coating method) result in a more efficient and effective approach than other modification methods. Finally, using graphene oxide as a support for biocidal metal nanoparticles provides an opportunity for the regeneration of biocidals after release. However, additional studies must be conducted to examine the in-situ regeneration of the GO/Ag nanocomposite to fully exploit this potential.

ASSOCIATED CONTENT

Supporting Information: FE-SEM and backscatter electron microscopy of (A) GO functionalized TFC and (B) GO/Ag nanocomposite functionalized TFC. Elements with high atomic numbers backscatter electrons more strongly than lighter elements with low atomic numbers and thus appear brighter on the image (Figure S.1). TEM images of (A) GO, (B) Ag NPs, and (C) GO/Ag nanocomposite (Figure S2). ATR-FTIR spectra of (A) a GO nanosheet and GO/Ag nanocomposite and (B) a control TFC and GO/Ag nanocomposite functionalized TFC membrane (Figure S3). The zeta potential of the surface of the pristine and functionalized membranes as a function of solution pH. Measurements were taken at room temperature (23°C) in a solution of 1 mM KCl by adjusting pH with the dropwise addition of HCl and NaOH (Figure S.4). Surface roughness properties of pristine and GO/Ag functionalized TFC FO membranes (Table S1). XPS results for (A) pristine membrane and (B) cysteamine treated TFC FO membranes. Peaks at 198 eV for Cl2P and 162 for Sulfor S2P are shown in (A) and (B), respectively (Figure S5). Elemental composition of the membrane surface of pristine and functionalized membranes before and after sonication (Table S2). The physical stability of the silver NPs on the Ag NP decorated and GO/Ag functionalized membranes from XPS results. A 7-min bath sonication was applied to the membranes, and the percent of silver on the membrane surface was estimated (Figure S6).

ACKOWLEDGMENTS

The authors acknowledge the Natural Sciences and Engineering Research Council (NSERC) of Canada for providing funding support for this project. Adel Soroush acknowledges the support of a graduate entrance scholarship from Concordia University, and Yule Silvino acknowledges the support from Science without Boarders, a Brazilian program for her summer internship at Concordia University.

Literature Cited

1. R. L. McGinnis and M. Elimelech, *Desalination*, 2007, **207**, 370-382.
2. M. Elimelech and W. A. Phillip, *Science*, 2011, **333**, 712-717.
3. A. Matin, Z. Khan, S. M. J. Zaidi and M. C. Boyce, *Desalination*, 2011, **281**, 1-16.
4. B. Mi and M. Elimelech, *Journal of Membrane Science*, 2010, **348**, 337-345.
5. M. F. Siddiqui, M. Rzechowicz, H.-S. Oh, N. Saeidi, L. J. Hui, H. Winters, A. G. Fane and T. H. Chong, *International Biodeterioration & Biodegradation*, 2015, **104**, 74-82.
6. P. Cristiani and G. Perboni, *Bioelectrochemistry*, 2014, **97**, 120-126.
7. T. M. D. Rana, *Chem. Rev*, 2010, **110**, 2448-2471.
8. G. D. Kang and Y. M. Cao, *Water Res*, 2012, **46**, 584-600.
9. S. Romero-Vargas Castrillón, X. Lu, D. L. Shaffer and M. Elimelech, *Journal of Membrane Science*, 2014, **450**, 331-339.
10. X. Lu, S. Romero-Vargas Castrillon, D. L. Shaffer, J. Ma and M. Elimelech, *Environ Sci Technol*, 2013, **47**, 12219-12228.
11. A. Asatekin, E. A. Olivetti and A. M. Mayes, *Journal of Membrane Science*, 2009, **332**, 6-12.
12. S. K. Atar Adout , Ayse Asatekin, Anne M. Mayes and Menachem Elimelech *environmental Science & Technology*, 2010, **44**, 2406–2411.
13. A. Tiraferri, Y. Kang, E. P. Giannelis and M. Elimelech, *ACS Appl Mater Interfaces*, 2012, **4**, 5044-5053.
14. A. Nguyen, L. Zou and C. Priest, *Journal of Membrane Science*, 2014, **454**, 264-271.
15. Y. Gao, M. Hu and B. Mi, *Journal of Membrane Science*, 2014, **455**, 349-356.
16. A. Tiraferri, C. D. Vecitis and M. Elimelech, *ACS applied materials & interfaces*, 2011, **3**, 2869-2877.
17. C. D. Vecitis, M. H. Schnoor, M. S. Rahaman, J. D. Schiffman and M. Elimelech, *Environ Sci Technol*, 2011, **45**, 3672-3679.
18. I. Sawada, R. Fachrul, T. Ito, Y. Ohmukai, T. Maruyama and H. Matsuyama, *Journal of Membrane Science*, 2012, **387-388**, 1-6.
19. K. Zodrow, L. Brunet, S. Mahendra, D. Li, A. Zhang, Q. Li and P. J. Alvarez, *Water Res*, 2009, **43**, 715-723.
20. J. Yin, Y. Yang, Z. Hu and B. Deng, *Journal of Membrane Science*, 2013, **441**, 73-82.
21. G. P. b. P. Cristiani a, *Bioelectrochemistry*, 2014, **97**, 120-126.
22. O. C. Compton and S. T. Nguyen, *Small*, 2010, **6**, 711-723.
23. Y. Zhu, S. Murali, W. Cai, X. Li, J. W. Suk, J. R. Potts and R. S. Ruoff, *Adv Mater*, 2010, **22**, 3906-3924.
24. B. Mi, *Science*, 2014, **343**, 740-742.
25. R. K. Joshi, P. Carbone, F. C. Wang, V. G. Kravets, Y. Su, I. V. Grigorieva, H. A. Wu, A. K. Geim and R. R. Nair, *Science*, 2014, **343**, 752-754.
26. K. Celebi, J. Buchheim, R. M. Wyss, A. Droudian, P. Gasser, I. Shorubalko, J. I. Kye, C. Lee and H. G. Park, *Science*, 2014, **344**, 289-292.
27. W. Choi, J. Choi, J. Bang and J. H. Lee, *ACS Appl Mater Interfaces*, 2013, **5**, 12510-12519.
28. X. Huang, X. Qi, F. Boey and H. Zhang, *Chemical Society reviews*, 2012, **41**, 666-686.
29. M. R. Das, R. K. Sarma, R. Saikia, V. S. Kale, M. V. Shelke and P. Sengupta, *Colloids Surf B Biointerfaces*, 2011, **83**, 16-22.
30. C. Li, X. Wang, F. Chen, C. Zhang, X. Zhi, K. Wang and D. Cui, *Biomaterials*, 2013, **34**, 3882-3890.

31. A. F. de Faria, D. S. Martinez, S. M. Meira, A. C. de Moraes, A. Brandelli, A. G. Filho and O. L. Alves, *Colloids Surf B Biointerfaces*, 2014, **113**, 115-124.
32. I. Ocsoy, M. L. Paret, M. A. Ocsoy, S. Kunwar, T. Chen, M. You and W. Tan, *ACS Nano*, 2013, **7**, 8972-8980.
33. J. H. F. Thierry Cassagneau, *J. Phys. Chem. B*, 1999, **103**, 1789-1793.
34. M. S. Rahaman, H. Thérien-Aubin, M. Ben-Sasson, C. K. Ober, M. Nielsen and M. Elimelech, *Journal of Materials Chemistry B*, 2014, **2**, 1724.
35. M. S. Mauter, Y. Wang, K. C. Okemgbo, C. O. Osuji, E. P. Giannelis and M. Elimelech, *ACS Appl Mater Interfaces*, 2011, **3**, 2861-2868.
36. P. Madhavan, P. Y. Hong, R. Sougrat and S. P. Nunes, *ACS Appl Mater Interfaces*, 2014, **6**, 18497-18501.
37. Z. Zhu, M. Su, L. Ma, L. Ma, D. Liu and Z. Wang, *Talanta*, 2013, **117**, 449-455.
38. S. Vijay Kumar, N. M. Huang, H. N. Lim, A. R. Marlinda, I. Harrison and C. H. Chia, *Chemical Engineering Journal*, 2013, **219**, 217-224.
39. F. Perreault, M. E. Tousley and M. Elimelech, *Environmental Science & Technology Letters*, 2014, **1**, 71-76.
40. R. E. O. W.S. Hummers, *J. Am. Chem. Soc.*, 1958, **80**, 1339.
41. T. Y. Cath, M. Elimelech, J. R. McCutcheon, R. L. McGinnis, A. Achilli, D. Anastasio, A. R. Brady, A. E. Childress, I. V. Farr, N. T. Hancock, J. Lampi, L. D. Nghiem, M. Xie and N. Y. Yip, *Desalination*, 2013, **312**, 31-38.
42. R. N. Wenzel, *J. Phys. Chem*, 1949, **53**, 1466-1467.
43. G. Hurwitz, G. R. Guillen and E. M. V. Hoek, *Journal of Membrane Science*, 2010, **349**, 349-357.
44. S. B. Sharon L. Walker, Eric M. V. Hoek, and and M. Elimelech, *Langmuir*, 2002, **18**, 2193-2198.
45. J. U. Lee, W. Lee, S. S. Yoon, J. Kim and J. H. Byun, *Applied Surface Science*, 2014, **315**, 73-80.
46. J. Tian, S. Liu, Y. Zhang, H. Li, L. Wang, Y. Luo, A. M. Asiri, A. O. Al-Youbi and X. Sun, *Inorganic chemistry*, 2012, **51**, 4742-4746.
47. S. H. Eric M. Vrijenhoek , Menachem Elimelech, *journal of Membrane Science*, 2001, **185**, 115-128.
48. W.-P. Xu, L.-C. Zhang, J.-P. Li, Y. Lu, H.-H. Li, Y.-N. Ma, W.-D. Wang and S.-H. Yu, *Journal of Materials Chemistry*, 2011, **21**, 4593.
49. Y. Li, H. Yuan, A. von dem Bussche, M. Creighton, R. H. Hurt, A. B. Kane and H. Gao, *Proc Natl Acad Sci U S A*, 2013, **110**, 12295-12300.
50. W. R. Li, X. B. Xie, Q. S. Shi, H. Y. Zeng, Y. S. Ou-Yang and Y. B. Chen, *Appl Microbiol Biotechnol*, 2010, **85**, 1115-1122.
51. M. L. P. Ismail Ocsoy, Muserref Arslan Ocsoy, Sanju Kunwar, Tao Chen, Weihong Tan, Mingxu You,, *ACS Nano*, 2013, **7**, 8972-8990.
52. S. Romero-Vargas Castrillón, F. Perreault, A. F. de Faria and M. Elimelech, *Environmental Science & Technology Letters*, 2015, **2**, 112-117.

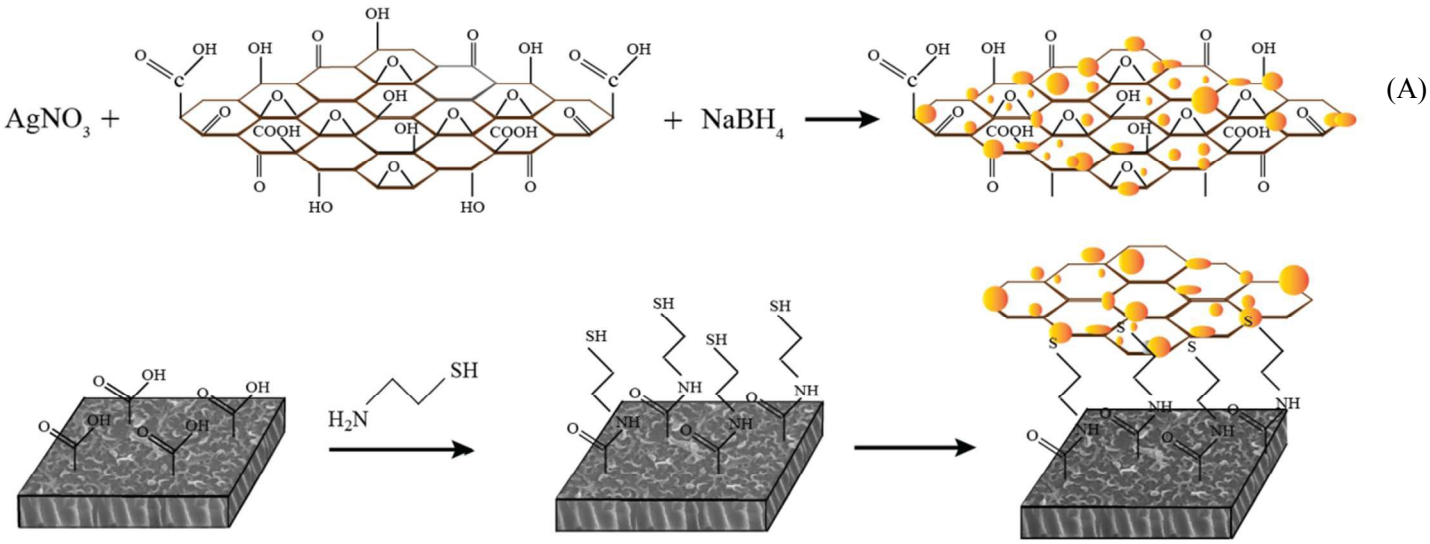

Scheme 1. Covalently bonded AgNP-decorated GO nanosheets through click chemistry on TFC FO membranes: (A) in situ AgNPs synthesized onto the GO nanosheets, (B) amide forming reaction and thiol functionalization of the TFC FO membrane, and (C) covalent binding of the GO/Ag nanocomposite to the TFC FO membrane surface.

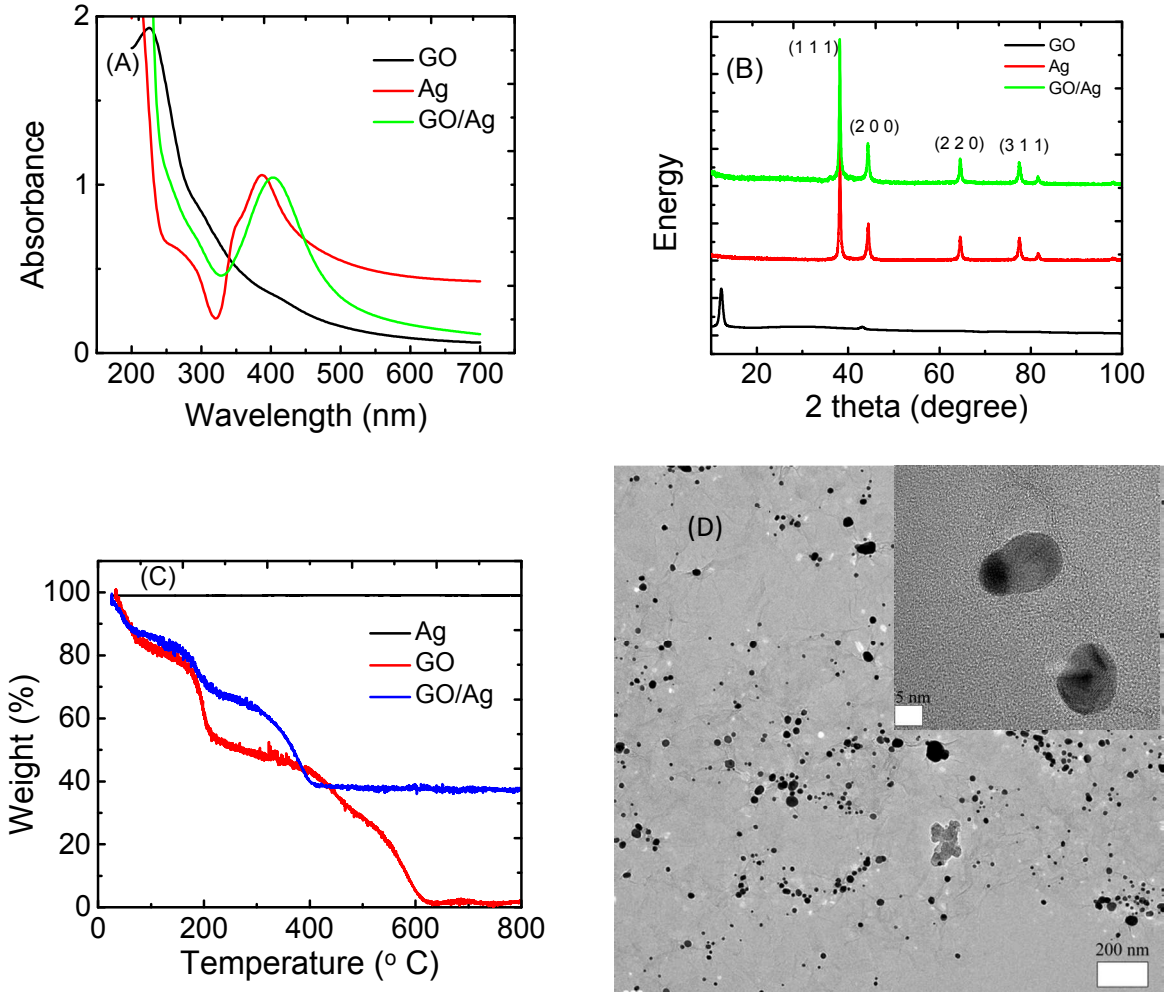

Figure 1. Characterization of the GO/Ag nanocomposite. (A) UV-Vis spectra, (B) XRD patterns, (C) thermogravimetric curves for Ag NPs, GO nanosheets, and GO/Ag nanocomposites, and (D) HR-TEM images of the GO/Ag nanocomposite.

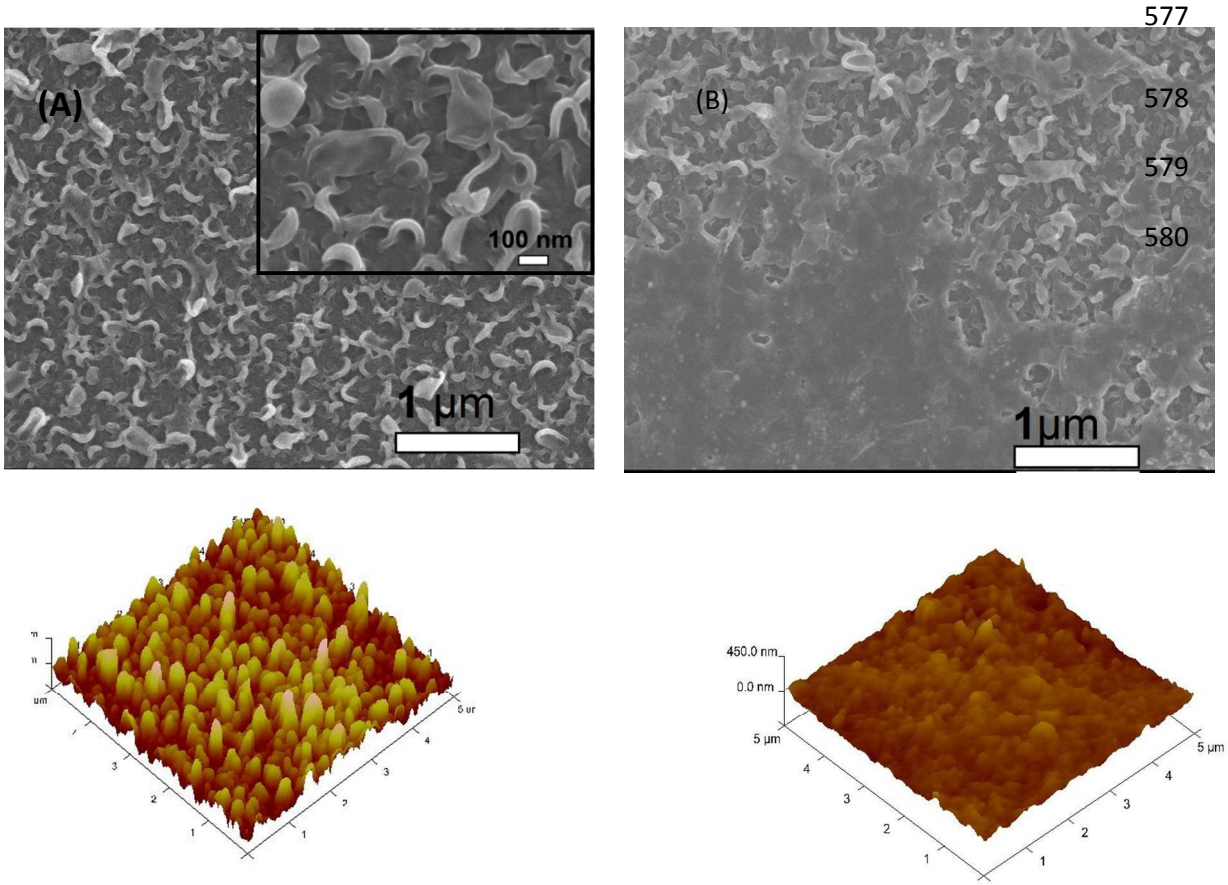

(C) (D)

Figure 2. FESEM images of (A) the polyamide active layer of the TFC membrane and (B) the GO/Ag functionalized polyamide active layer of the TFC membrane. AFM images of (C) the TFC membrane and (D) the GO/Ag functionalized TFC membrane.

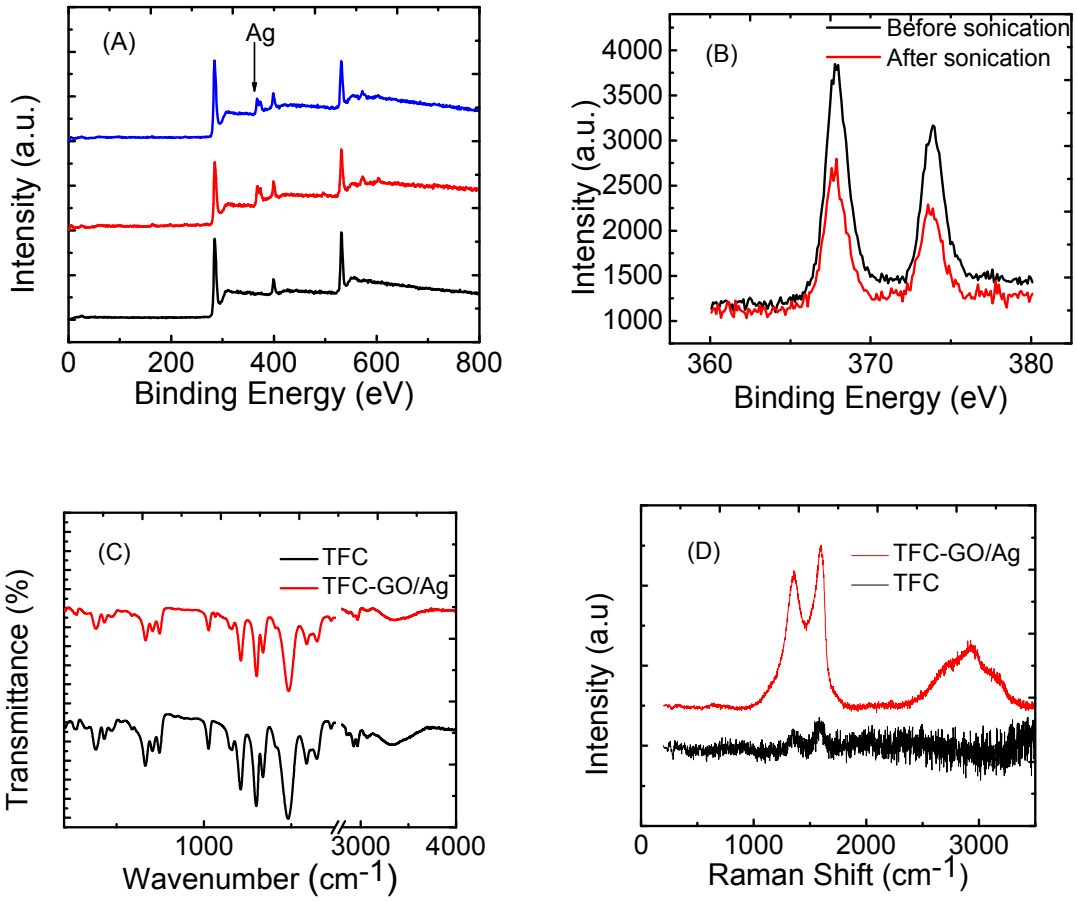

Figure 3. Surface characterization of virgin and functionalized TFC FO membranes: (A) XPS analysis of the TFC (black), GO/Ag nanocomposite functionalized membranes before (red) and after (blue) sonication, (B) XPS analysis at a higher magnification, (C) ATR-FTIR spectra of the virgin and functionalized TFC membranes, and (D) Raman spectra of the control and functionalized TFC membranes.

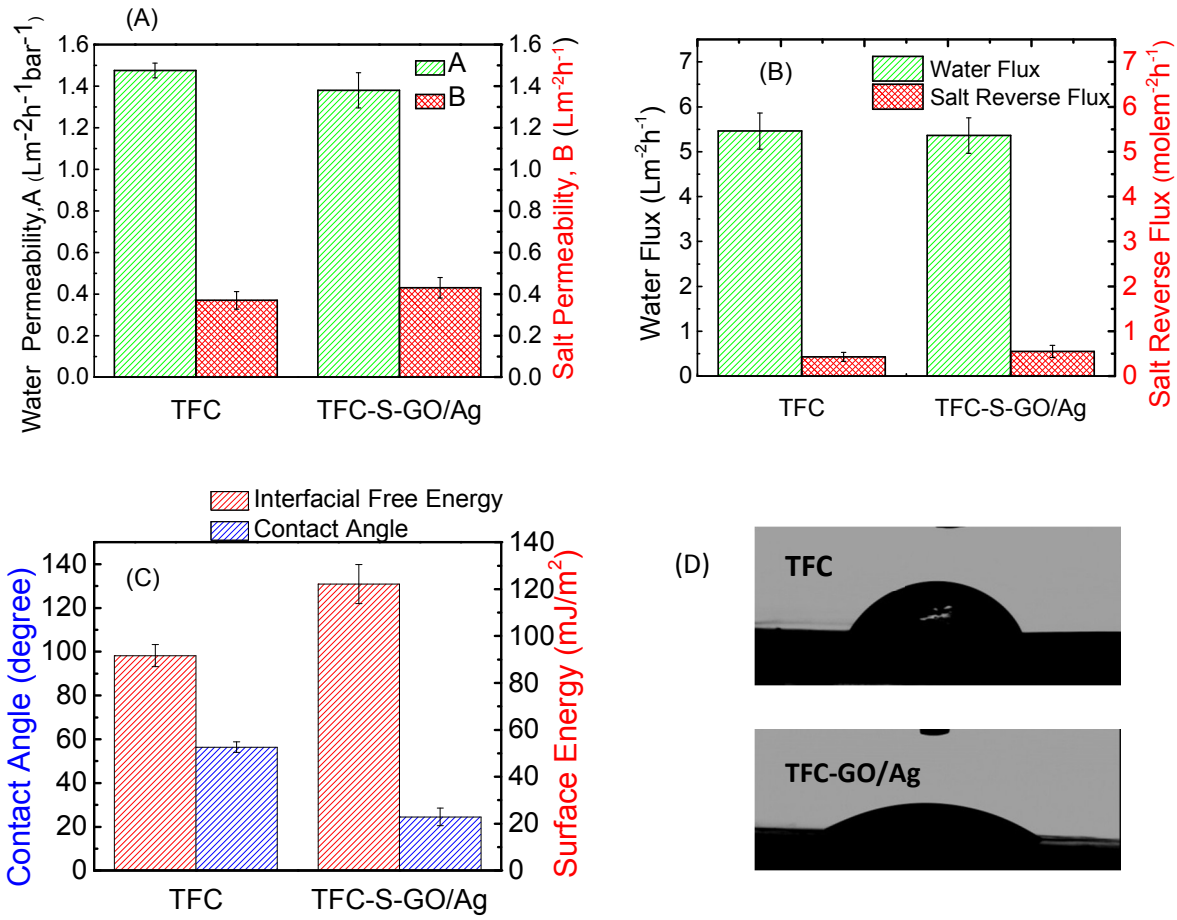

Figure 4. Membrane properties before and after modification. (A) The water permeability and salt permeability of the TFC and GO/Ag functionalized TFC membranes (in the RO mode). (B) The water flux and salt reverse flux (in the FO mode) of the TFC and GO/Ag functionalized TFC membranes. (C) The water contact angle of the TFC and GO/Ag functionalized TFC membranes. (D) Water droplets on the TFC and GO/Ag functionalized TFC membrane surfaces.

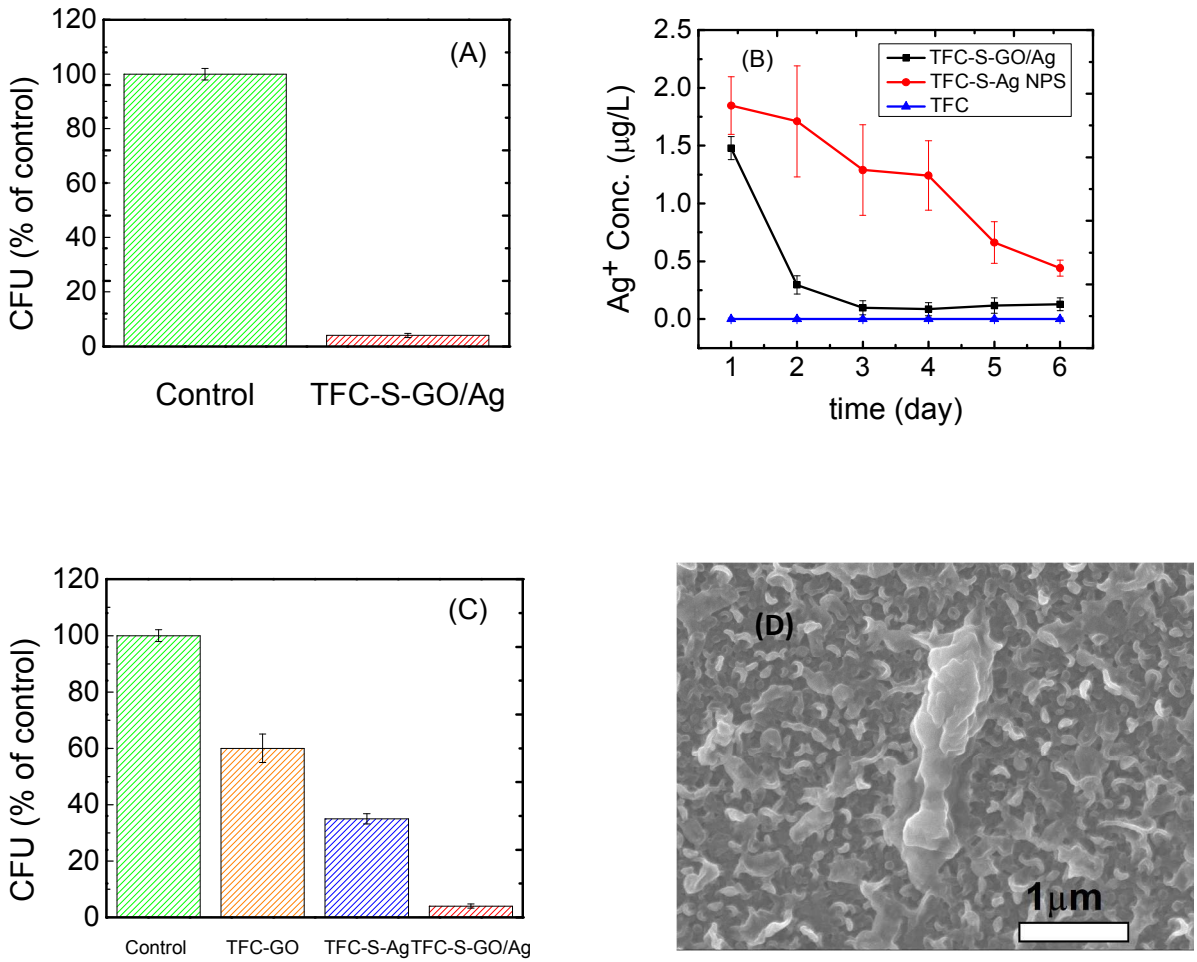

Figure 5. Colony-forming units (CFU) after *E. coli* cells had been in contact with the control and GO/Ag functionalized membranes for 1 h at room temperature: (A) CFU for the virgin and GO/Ag functionalized membranes, (B) the silver ion release rate from the GO/Ag functionalized membranes, (C) CFU for the virgin, GO, AgNPs, and GO/Ag functionalized TFC membranes, and (D) an SEM image of the inactivated bacteria on the GO/Ag functionalized TFC membrane.